A case study of azimuthal AVO analysis with anisotropic spreading correction

Xiaoxia Xu and Ilya Tsvankin, Colorado School of Mines, Golden, USA

Geomechanical properties of tight, low-porosity reservoirs are largely governed by natural fracture networks. Hence, reliable estimation of fracture density and orientation is extremely important for cost-effective hydraulic completion and hydrocarbon production. Direct information about fracturing can be obtained using borehole methods, such as image log analysis, which provide estimates of fracture counts and orientations on various scales. The main shortcoming of borehole measurements is that they are sensitive only to formation properties in the immediate vicinity of the well. In some cases, the spatial distribution of fractures can be inferred from fault maps obtained by coherence analysis of surface seismic data. However, the correlation between areas of high fracture density and fault locations is not always straightforward.

Therefore, fracture characterization increasingly relies on seismic inversion methods that operate with both 3D wide-azimuth surface data and VSP (vertical seismic profiling) surveys (Hall and Kendall, 2003; Gray and Todorovic-Marinic, 2004). In particular, valuable information about fracture orientation and density is provided by the azimuthal variation of such P-wave signatures as moveout attributes and amplitude-variation-with-offset (AVO) response (Grechka and Tsvankin, 1999; Lynn et al., 1999; Bakulin et al., 2000; Rüger, 2001; Neves et al., 2003). After cross-validation with borehole measurements, fracture maps obtained from azimuthal seismic attributes can serve as the input into reservoir simulation.

Both azimuthal AVO (often abbreviated as AVAZ) and moveout analysis have their advantages and drawbacks. While the AVO response provides local, high-resolution information about fracturing at the top or bottom of the reservoir, moveout attributes (e.g., the NMO ellipse) depend on the average fracture properties for the whole reservoir layer. When combined together, azimuthal AVO and moveout attributes can offer improved understanding of the spatial distribution and physical properties of fractures.

From the processing standpoint, azimuthal moveout measurements usually are more robust and less distorted by standard preprocessing algorithms. On the other hand, reflection amplitudes are more sensitive to the presence of anisotropy and can provide higher vertical resolution, which is especially important for thin reservoirs. In addition to the difficulties caused by the near surface (e.g., statics errors and coupling problems), both moveout and amplitude methods have to account for the propagation phenomena in the overburden. Interval NMO ellipses are obtained by applying the generalized Dix equation to the reflections from the top and bottom of the reservoir (Grechka et al. 1999; Neves et al., 2003). This procedure becomes unstable if the thickness of the reservoir layer is relatively small compared to its depth. Then, for purposes of moveout analysis it may become necessary to combine the reservoir with a layer above or below it.

It is less common in seismic fracture characterization to properly account for amplitude distortions in the overburden, in particular those caused by anisotropic geometrical spreading. The high sensitivity of geometrical spreading to the presence of anisotropy along the raypath can cause serious errors in AVO analysis (Rüger and Tsvankin, 1997; Tsvankin, 2005). To remove the geometrical-spreading factor and accurately estimate the reflection coefficient, Xu et al. (2005) and Xu and Tsvankin (2006a) developed a methodology of moveout-based anisotropic spreading correction (MASC). The moveout parameters that provide the input to MASC are obtained by 3D nonhyperbolic moveout inversion of wide-azimuth data (Vasconcelos and Tsvankin, 2006). It should be emphasized that MASC does not require any additional information about the velocity field and fits in a straightforward way into the processing flow of azimuthal AVO analysis. Synthetic tests on realistic orthorhombic layered models show that application of MASC becomes necessary when the azimuthal variation of the geometrical spreading reaches at least 1/3 of that of the reflection coefficient (Xu and Tsvankin, 2006b).

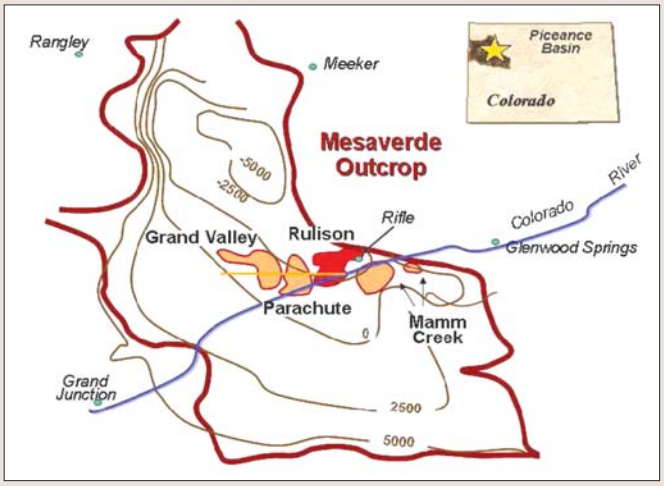

Figure 1. *Location of the Rulison Field in the Piceance Basin, Colorado.*

Here, we carry out azimuthal moveout and AVO analysis of P-wave data acquired above a fractured reservoir in the Rulison Field in Colorado. Prior to estimating the azimuthally varying AVO gradient, we apply MASC to correct reflection amplitudes for the geometrical spreading in the overburden. Comparison of our processing results for the bottom of the reservoir with those obtained with a conventional gain correction shows that MASC made it possible to enhance and focus one of the two major azimuthal AVO anomalies. Analysis of the AVO gradients at the top and bottom of the reservoir provides important insight into the fracture distribution and helps to identify zones of intense fracturing.

Geologic background. Rulison Field is a basin-centered gas accumulation in the south Piceance Basin, Garfield County, Colorado (Figure 1). Gas production comes primarily from the Williams Fork Formation, which consists of channel sand lenses embedded in fine-grained levee deposition (Figure 2). The reservoir is capped by the UMV shale, while the Cameo coal beneath the reservoir is believed to provide the source for the gas accumulation. The unconformity at the top of the Mesaverde group underlies a massive shale formation.

Table 1. *Acquisition parameters of the survey.*

Survey type	3D 9-C
Subsurface bin size	55' x 55'
Number of receiver locations	1500
Number of source locations	770
Receiver grid	110' inline spacing, 330' between lines
Source grid	110' inline spacing, 660' between lines
Receiver array	1, 3-C VectorSeis System Four
Source array	Mertz 18
P-wave sweep range	6-120 Hz

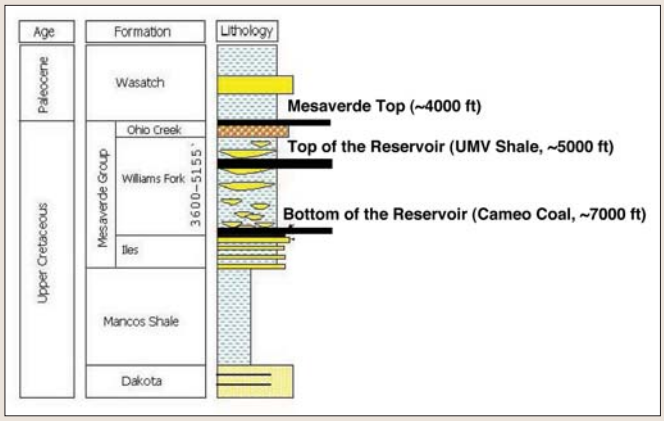

Figure 2. *Stratigraphic column of the Rulison Field. The gas-producing reservoir is bounded by the UMV shale and the Cameo coal. The Mesaverde Top is an unconformity that separates the Mesaverde group from the overlying Wasatch Formation.*

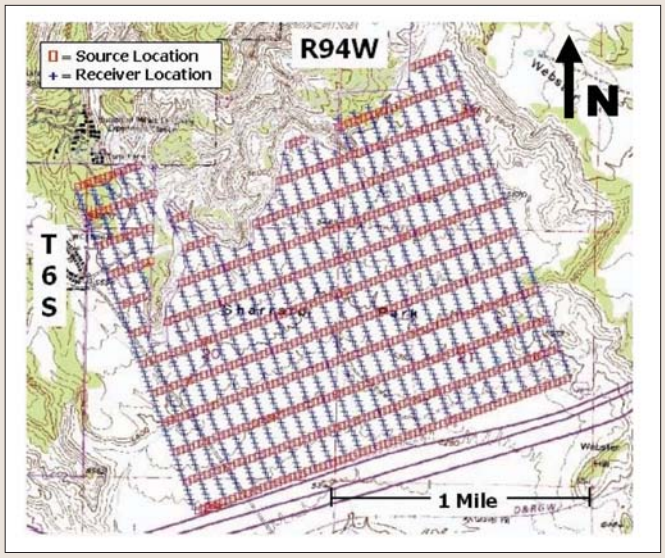

Figure 3. *Seismic acquisition grid for the RCP nine-component 2003 survey.*

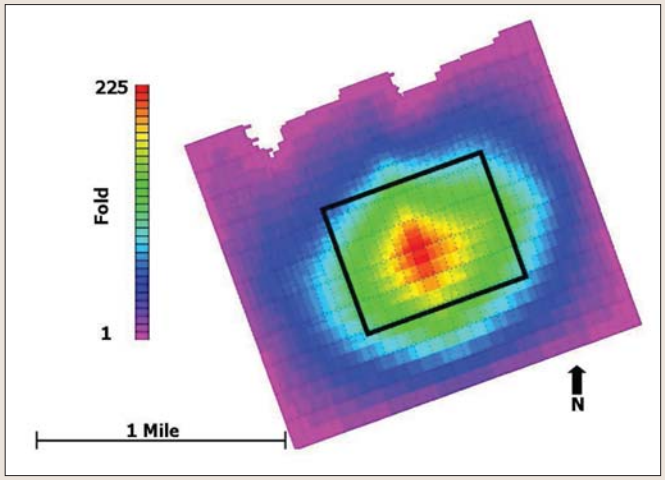

Figure 4. *P-wave fold for the 55 ×55 ft bin size. The square in the center marks the study area of this paper.*

The reservoir lithology is classified as tight sand with the matrix permeability on the order of microdarcies and porosity of 6–12%. The top several hundred feet of the reservoir formation are saturated with water, which is replaced by gas in the lower part of the reservoir (Cumella and Ostby, 2003). The pay section is relatively thick (about 1200 ft) and is considered to be normally pressured or slightly overpressured. Because of the low porosity and matrix permeability, characterization of natural fracture networks has vital importance for cost-effective development of the field.

Data acquisition and processing. To map the spatial distribution and orientation of fractures and study the in-situ stress field, the Reservoir Characterization Project (RCP) at CSM acquired a 3D multicomponent seismic survey over a 2.2 × 2.5 km area of the Rulison Field. The orthogonal acquisition geometry was designed to reach optimal balance between the uniformity of the azimuthal distribution and the layout economy (Figure 3). The data coverage is especially dense near the center of the survey area, with the highest fold of 225 for a small bin size of 55 × 55 ft (Table 1 and Figure 4). This data set served as the baseline survey for a time-lapse monitoring study conducted by RCP.

Prior to the AVO processing described below, a statics correction was applied to the data by Veritas. As illustrated by the cross-section in Figure 5, the data quality is above average for land surveys. Also, the subsurface structure is close to layer-cake, which simplifles application of azimuthal moveout and AVO analysis and the anisotropic geometrical-spreading correction (MASC).

To improve azimuthal and offset coverage, we collected CMP gathers into superbins. The choice of the superbin size is nontrivial and requires conducting a number of tests. Relatively small superbins suffer from nonuniformity of the distribution of offsets and azimuths; on the other hand, using large superbins increases the influence of lateral heterogeneity. After experimenting with several bin sizes, we found 5×5 superbins to be optimal. Further increase in size reduces semblance values in 3D moveout analysis, which is likely caused by lateral heterogeneity.

Figure 6 displays a 5×5 superbin gather in the upper left corner of the study area. The ground roll was suppressed using the slope filter suggested by Vasconcelos and Grechka (2007), which is designed to minimize azimuthal distortions. The same gather after application of azimuthally-varying NMO correction is shown in Figure 7. The bending at far offsets (i.e., a "hockey stick") for the reflection from the top of the reservoir (UMV shale) indicates the presence of nonhyperbolic moveout generated in the overburden.

The azimuthally-varying NMO velocity is described by a quadratic function of the horizontal coordinates and typically traces out an ellipse in the horizontal plane (Grechka and Tsvankin, 1998). Similarly, the azimuthal variation of

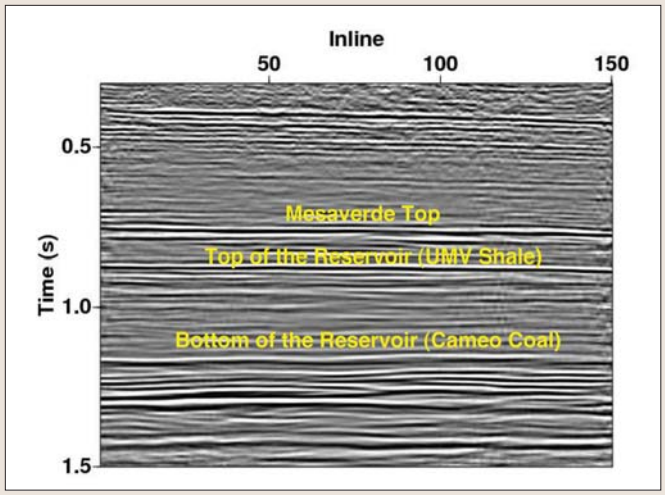

Figure 5. *Seismic section across the middle of the survey area. The reflectors analyzed in the paper are marked on the plot.*

AVO gradient can be approximated by an elliptical curve, unless the gradient changes sign with azimuth (Rüger, 2001). For laterally homogeneous models, the orientation and eccentricity of both ellipses depend on the direction, density, and fluid saturation of subsurface fracture systems. To reconstruct NMO and AVO ellipses, it is common to divide 3D data into azimuthal sectors and estimate the NMO velocity and AVO gradient in each sector separately. Although implementation of this approach is facilitated by application of existing 2D algorithms, it suffers from bias caused by uneven distribution of offsets and azimuths (Grechka and Tsvankin, 1999). Here, we adopted a more robust "global" algorithm that honors the azimuth of each trace and fits an ellipse to the data using all source-receiver pairs in a 3D CMP gather (Grechka and Tsvankin, 1999; Vasconcelos and Tsvankin, 2006).

An essential part of our processing sequence is azimuthal nonhyperbolic moveout analysis based on the algorithm of Vasconcelos and Tsvankin (2006) for layered orthorhombic or HTI (transversely isotropic with a horizontal symmetry axis) media. This algorithm is designed to estimate the effective P-wave moveout parameters, which include the orientation and semiaxes of the NMO ellipse and the "anellipticity" coefficients $\eta^{(1)}$, $\eta^{(2)}$, and $\eta^{(3)}$ (for parameter definitions, see Tsvankin, 2005).

Note that $\eta^{(1,2,3)}$ determine the azimuthally varying parameter η responsible for nonhyperbolic moveout on wide-azimuth gathers. The first step is to reconstruct the NMO ellipse from conventional-spread wide-azimuth data with the maximum offset-to-depth ratio close to unity. Second, this ellipse is used as the initial guess to carry out 3D nonhyperbolic moveout analysis of all traces in the gather and to estimate the full set of moveout parameters discussed above. These parameters not only allow us to flatten long-spread reflection events in the wide-azimuth gather, but also serve as the input to the geometrical-spreading correction. Third, we perform amplitude picking along the traveltime surface defined by the moveout parameters. Fourth, the picked amplitudes are corrected for the geometrical spreading using the method (MASC) of Xu and Tsvankin. Finally, the corrected amplitudes are inverted for the azimuthally-varying AVO gradient (along with the AVO intercept) to obtain the AVO ellipse. To evaluate the impact of the anisotropic spreading correction on the azimuthal AVO analysis, we also repeated the last two processing steps with MASC replaced by the conventional t^2 gain.

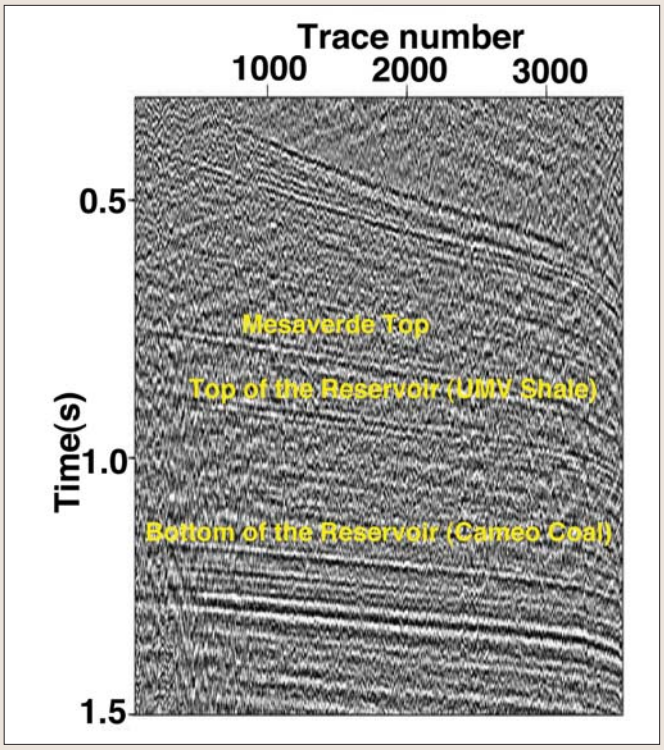

Figure 6. *CMP supergather in the upper left corner of the study area. The maximum offset is 7700 ft.*

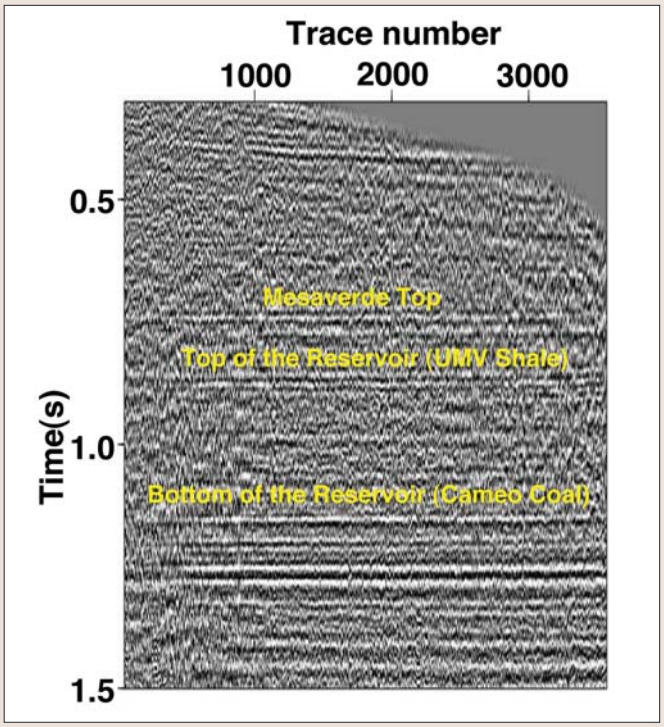

Figure 7. *Supergather from Figure 6 after application of azimuthally-varying hyperbolic moveout correction. The maximum offset-to-depth ratio for the top of the reservoir (UMV shale) is 1.5.*

The azimuthal moveout and AVO analyses were carried out for CMP locations inside a square area in the center of the RCP survey (Figure 4), where the fold per superbin varied from 1500 to 5000. Figure 8 shows the azimuthal and offset coverage for CMP superbins in the four corners of this study area; the coverage increases toward the center of the survey. It is evident that uniform azimuthal coverage, which

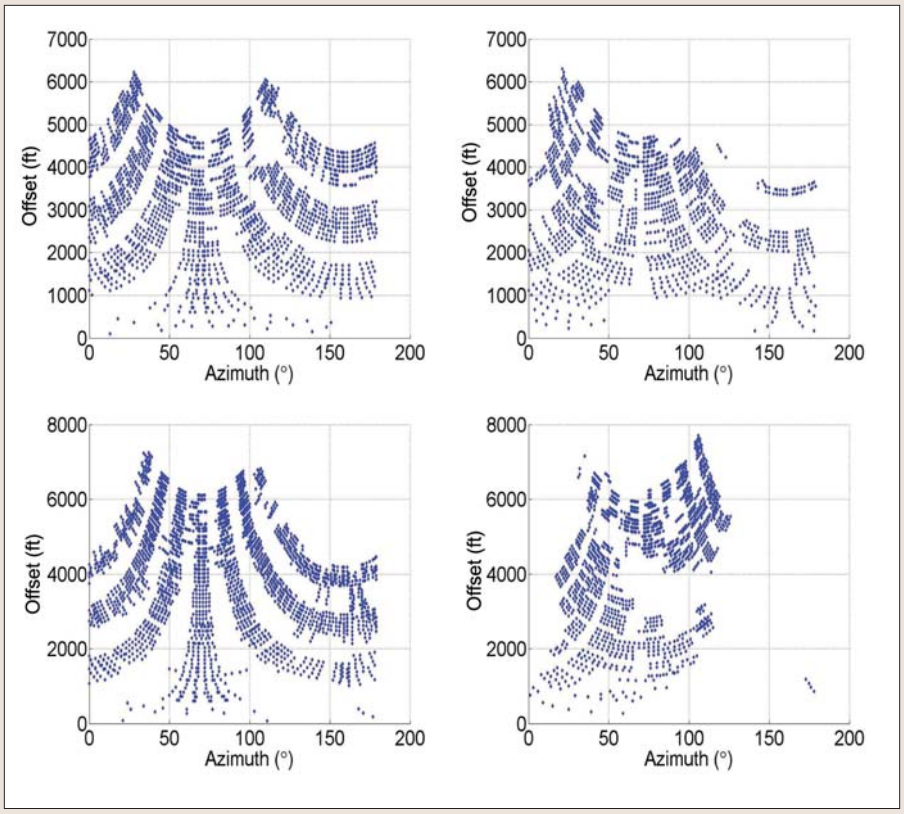

Figure 8. *Distribution of offsets and azimuths for CMP superbins in the four corners of the study area. Note that full azimuthal coverage is achieved for offsets up to about 5000 ft.*

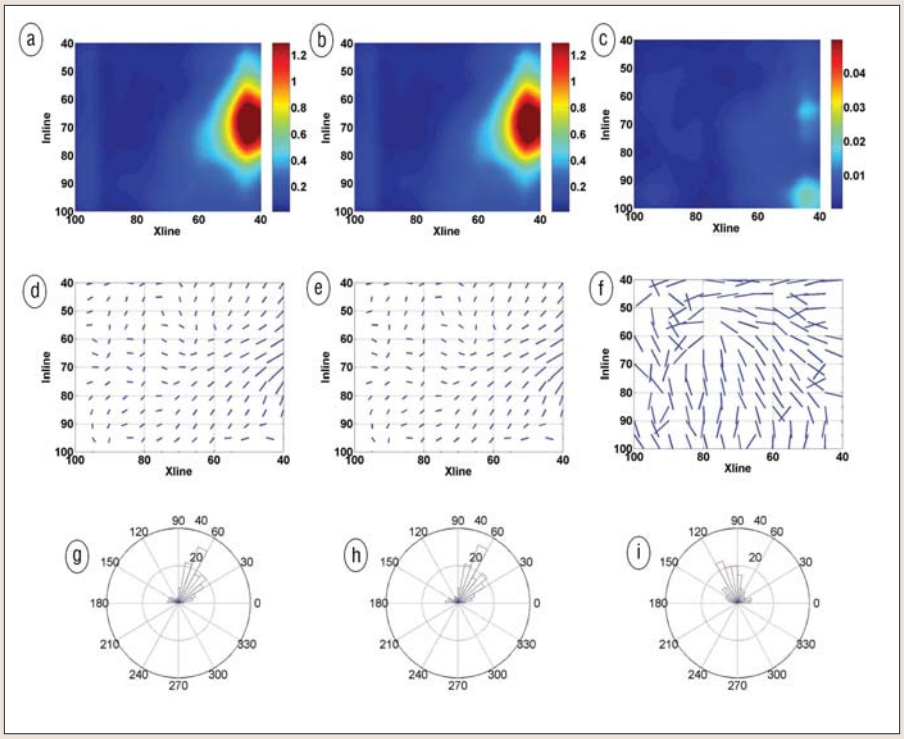

Figure 9. *AVO and NMO ellipses estimated for the reflection from the Mesaverde Top. The first two columns display the AVO ellipses computed using MASC (left) and the conventional t^2 gain correction (center). The right column shows the effective NMO ellipses. The top row (panels a, b, and c) is the eccentricity of the ellipses calculated by subtracting unity from the ratio of the semi-major and semi-minor axes; the semi-major axis of the AVO ellipse corresponds to the larger absolute value of the AVO gradient. The middle row (panels d, e, and f) is the azimuth of the semimajor axis; the length of the ticks is proportional to the eccentricity. Panels g, h, and i (bottom row) are the rose diagrams of the azimuths from panels d, e, and f, respectively. The azimuths in the middle and bottom rows are computed with respect to the north.*

is critical for our processing, extends to offsets of about 5000 ft. This implies that the NMO and AVO ellipses for the Mesaverde top and the top of the reservoir should be largely free from acquisition-related bias. The processing results for the bottom of the reservoir (Cameo coal), however, may bear some acquisition footprint, particularly at the edges of the study area.

Results of azimuthal seismic analysis. Here, we discuss azimuthal AVO and NMO analysis for three major reflectors: the top of the Mesaverde group, the top of the reservoir (UMV shale), and the bottom of the reservoir (Cameo coal). To minimize possible edge effects, some processed CMP superbins included source/receiver locations outside of the study area in Figure 4. Both AVO and NMO ellipses are represented by their eccentricity and the orientation (azimuth) of the semi-major axis computed for each common midpoint.

Mesaverde Top. The AVO ellipses for the Mesaverde Top exhibit a distinctive azimuthal AVO anomaly near the east boundary of the study area (Figures 9a and 9b). The eccentricity of the ellipses is defined as the ratio of the semi-major and semi-minor axes minus unity. Therefore, at the center of this anomaly the AVO gradient in one principal azimuthal direction is more than twice as large as in the orthogonal direction. In contrast, the NMO ellipticity for this reflector is negligible, which suggests that the overburden is effectively azimuthally isotropic with respect to NMO velocity. The axes of the AVO ellipses in the area of the anomaly have azimuths close to 45° and 135°. Since the reflection coefficient responds to the local changes of rock properties at the interface, the azimuthal AVO anomaly in Figure 9 may be associated with an intensely fractured zone near the Mesaverde Top. The obtained AVO-gradient map offers potentially valuable information for the operating company, which is interested in using formations above the Mesaverde Top to store production water.

Although the anellipticity parameter η estimated from nonhyperbolic moveout inversion is substantial (0.15 on average), it is almost the same in both vertical symmetry planes of the medium (Figure 10b). On the whole, the reflection moveout and, consequently, geometrical spreading for the Mesaverde Top is weakly dependent on azimuth (Figure 10a). Comparison

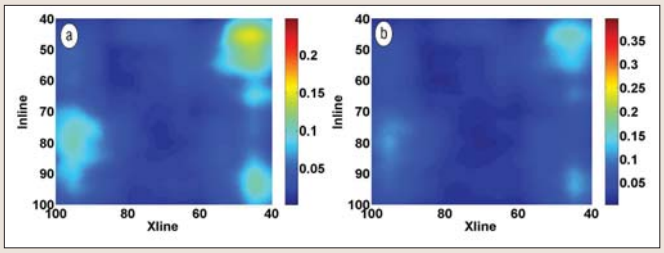

Figure 10. *Azimuthal variation of the (a) geometrical spreading and (b) effective anellipticity parameter η for the Mesaverde Top. Plot (a) shows the relative difference between the spreading values in the vertical symmetry planes for the offset-to-depth ratio equal to one; the symmetry planes correspond to the axes of the NMO ellipse. Plot (b) shows the difference between the parameters $\eta^{(1)}$ and $\eta^{(2)}$ defined in the vertical symmetry planes of the medium.*

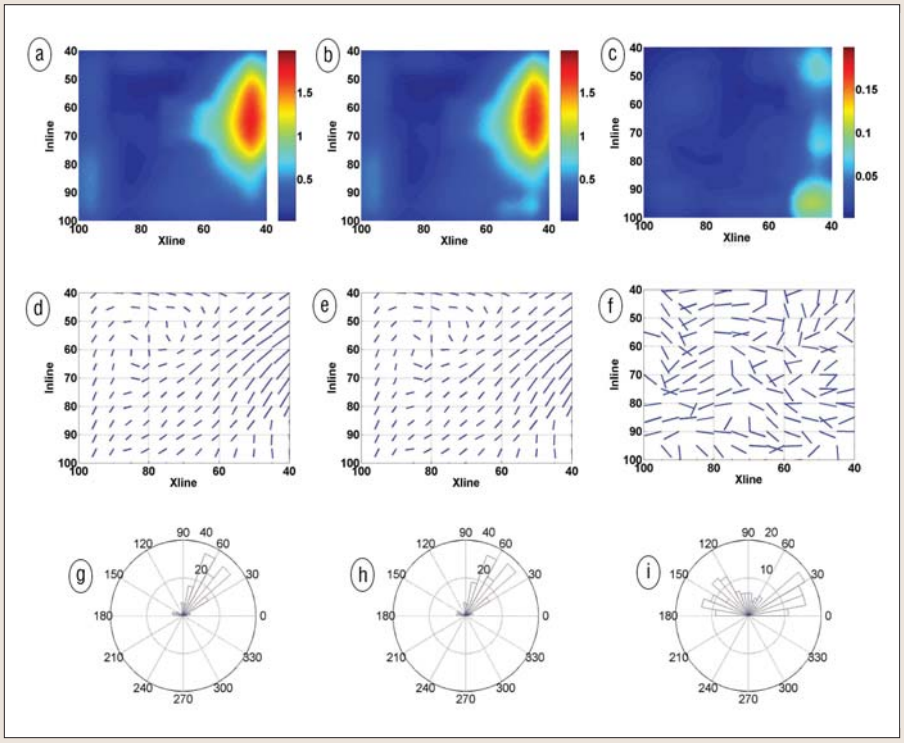

Figure 11. *AVO ellipses for the top of the reservoir (left and center columns) and the interval NMO ellipses in the UMV shale (right column; same display as in Figure 9).*

of the first two columns of Figure 9 confirms that the impact of MASC (i.e., of the anisotropic spreading correction) on the azimuthal AVO response for the Mesaverde Top is small.

Top of the reservoir (UMV shale). Similar to the Mesaverde Top, the only pronounced AVO-gradient anomaly at the top of the reservoir is near the east boundary of the study area (Figure 11a). The magnitude of this anomaly, however, is about 30% higher than that for the Mesaverde Top, and the point of the maximum AVO ellipticity is shifted up by about 200 m. Since the UMV shale layer above the reservoir is likely to be transversely isotropic with a vertical symmetry axis (VTI; see below), the anomaly in Figure 11 may be caused by a "soft spot" of high fracture density in the upper reservoir. The influence of the anisotropic spreading correction on the azimuthal AVO response at the top of the reservoir is marginal for the same reason as for the Mesaverde Top.

The maximum effective NMO ellipticity for the top of the reservoir is only slightly larger than that for the Mesaverde Top. The right column in Figure 11 shows the interval NMO ellipses in the UMV shale layer computed from the generalized Dix equation of Grechka et al. (1999). The orientations of the ellipses are almost random, which suggests that the shale formation is either azimuthally isotropic or not thick enough for the layer-stripping operation to be sufficiently stable.

Bottom of the reservoir (Cameo coal). The azimuthal seismic attributes for the bottom of the reservoir are shown in Figure 12. Two significant AVO-gradient anomalies appear in the upper right and lower left corners of the study area (Figures 12a,b). The magnitude of both anomalies is close to 1.5, which means that the semi-major axis of the AVO ellipse is 2.5 times larger than the semi-minor axis by absolute value. The azimuth of the semi-major axis (Figure 12) exhibits a strikingly regular pattern that might be related to the geomechanical processes that produce wrenching faults in the area (Jansen, 2005).

According to the AVO results in Figures 12g and 12h, the average fracture azimuth at the bottom of the reservoir should be close to N70W. The large thickness of the reservoir ensures stable computation of the interval NMO ellipses (the right column in Figure 12). The only noticeable azimuthal NMO anomaly is in the upper right corner of the area and partially overlaps with one of the azimuthal AVO anomalies described above. The magnitude of the NMO anomaly is close to 8%, which translates into a difference of about 0.08 between the anisotropy parameters $\delta^{(1)}$ and $\delta^{(2)}$ in the vertical symmetry planes (see Tsvankin, 2005).

In contrast to the results for the more shallow reflectors, the anisotropic spreading correction (MASC) makes a significant impact on the azimuthal AVO response for the bottom of the reservoir (compare Figures 12a and 12b). The AVO anomaly in the lower left corner of the study area becomes much more pronounced and spatially coherent after application of MASC. The strong azimuthal variation of the geometrical spreading in the lower part of the area is likely caused by the influence of subvertical fractures in the thick reservoir formation (Figure 13). Therefore, the anisotropic spreading correction is essential for computing an accurate AVO response from the bottom of the reservoir. The contribution of MASC is smaller for the second AVO anomaly (Figures 12a and 12b), probably because of the more limited vertical extent of fracturing near the right boundary of the area.

Most existing case studies of azimuthal AVO analysis are conducted for the top of the reservoir formation (e.g., Neves et al. 2003). Using synthetic modeling for fractured gas sands, Sayers and Rickett (1997) concluded that the bottom of the reservoir often produces a stronger azimuthal AVO anomaly. However, since Sayers and Rickett (1997) did not apply an anisotropic spreading correction, their modeled amplitudes should have been influenced by both the reflection coefficient and the azimuthally varying geometrical spreading inside the reservoir. Our results demonstrate that to take full advantage of the azimuthal AVO signature of events reflected beneath the reservoir, it is critically important to remove the anisotropic geometrical-spreading factor from the recorded amplitudes. In addition, analysis of geometrical spreading

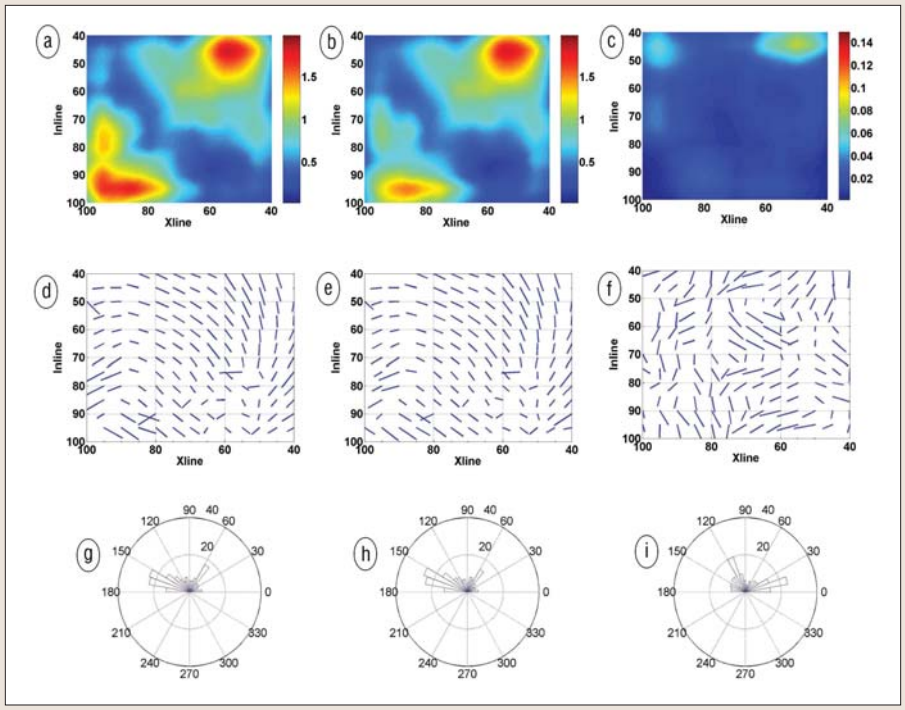

Figure 12. AVO ellipses for the bottom of the reservoir (left and center columns) and the interval NMO ellipses in the reservoir (right column; same display as in Figure 9).

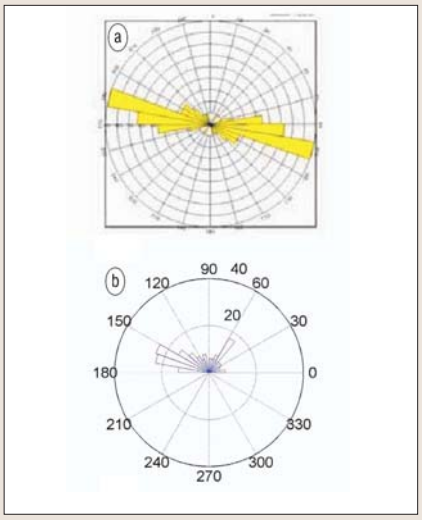

Figure 15. Rose diagrams of the fracture orientation obtained from EMI logs and azimuthal AVO analysis. The fracture directions were (a) counted in well RWF 542-20 within the reservoir; (b) estimated from the AVO ellipses at the bottom of the reservoir (Figure 12g).

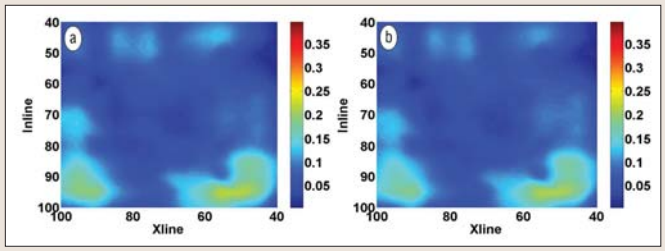

Figure 13. Azimuthal variation of the (a) geometrical spreading and (b) effective parameter η for the bottom of the reservoir (same display as in Figure 10).

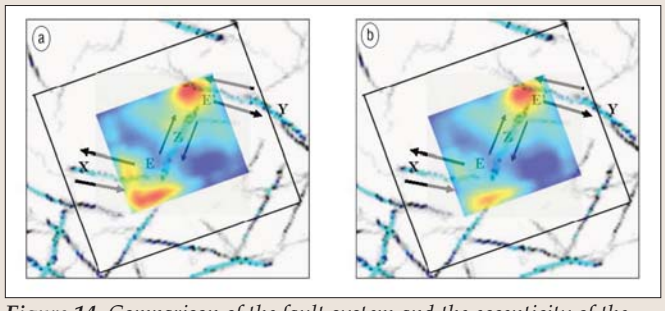

Figure 14. Comparison of the fault system and the eccenticity of the AVO ellipses for the bottom of the reservoir. The faults (blue lines), which are identical on plots (a) and (b), were mapped by Jansen (2005) using poststack P-wave images; the arrows indicate the slip movement. The azimuthal AVO attribute on plot (a) is computed using MASC (Figure 12a), and on plot (b) using the conventional spreading correction (Figure 12b). The black rectangle marks the RCP survey area. The AVO anomalies on plot (a) coincide with the intersections E and E′ of the two wrenching fault systems.

and input moveout parameters provides useful supplementary information for fracture characterization.

Discussion. In this section, we compare our processing results with available geologic and borehole information, estimate errors in the NMO velocities and AVO gradients, examine the correlation between the NMO and AVO ellipses, and outline some directions of future work.

Comparison with the fault distribution and EMI logs. Since both fractures and faults respond to subsurface stress fields, enhanced fracture zones are often associated with fault locations. It is, therefore, interesting to compare our fracture-characterization results with the fault distribution in the Rulison Field. Cumella and Ostby (2003) suggest that faults in the area follow a wrenching pattern. Employing the wrenching fault model, Jansen (2005) carried out fault mapping by applying automated curvature measurements to poststack P-wave images.

The primary fault system at the bottom of the reservoir is aligned along N70W, which agrees with the average azimuth of the semi-major axis of the AVO ellipse, while secondary stepover faults trend along N30E (Figure 14). Interestingly, the AVO-gradient anomalies obtained after application of MASC are located at the intersections of the two wrenching fault systems, where stress concentration is likely to induce intense fracturing. Also, the orientation of the AVO ellipses (Figures 12d and 12e) exhibits a rotation pattern, which seems to support the wrenching fault model.

An electrical microimager (EMI) log is available in well RWF 542-20 in the center of our study area. Figure 15 compares the fracture directions obtained from the EMI log and the azimuthal AVO analysis for the bottom of the reservoir. The difference between the dominant fracture orientations estimated from the two methods is less than 10°.

Acquisition footprint. Since full azimuthal coverage is achieved for offsets up to approximately 5000 ft, the NMO and AVO ellipses at the Mesaverde Top and the top of the reservoir (UMV shale) should not be distorted by the acquisition footprint. The azimuthal signatures for the bottom of the reservoir (Cameo coal) might be biased toward the dominant acquisition directions from 40° to 100°. The orientation of neither AVO nor NMO ellipses for the bottom of the reservoir, however, exhibits any noticeable bias (Figures 12d to 12f). In

particular, the azimuths of the AVO ellipses are practically random in the lower right corner of the area where the AVO eccentricity is small (Figures 12d and 12e). The absence of the acquisition footprint can be explained by the orthogonality of the acquisition layout, which ensures that 80% of all traces fall into the offset range with complete azimuthal coverage.

Error analysis. Assuming that the uncertainty in traveltime picking does not exceed 8 ms, Vasconcelos and Grechka (2007) estimated the variance in the estimated NMO velocities to be close to 7%. The most serious problem in the estimation of the NMO ellipses, however, is the bias caused by varying superbin size. The NMO ellipticity systematically increases over the area when the superbin size changes from 5×5 to 9×9. Since this increase in ellipticity is accompanied by lower semblance values, the larger superbins seem to be more influenced by lateral heterogeneity. On average, the semblance value for the top of the reservoir decreases from around 0.6 for 5×5 superbins to 0.45 for 9×9 superbins, while the effective NMO ellipticity increases by 0.04. Evidently, the 5×5 superbins used in our processing produce more reliable azimuthal seismic attributes.

The confidence interval for the eccentricity of the AVO ellipse can be inferred from the correlation between the magnitude of the AVO anomalies and the regularity of the ellipse orientation (Figures 9, 11, and 12). When the eccentricity is smaller than 0.3, the azimuths of the AVO ellipses are random, which is particularly clear in the upper left quarter of Figure 11d and the lower right quarter of Figure 12d. The AVO azimuths show a more regular pattern for eccentricities exceeding 0.3. Since AVO ellipses are estimated independently at each CMP location with no data overlap between adjacent gathers and no smoothing, the confidence level of the AVO eccentricity can be set at 0.3. The magnitude of the major azimuthal AVO anomalies at the bottom of the reservoir is five times this confidence level.

Since the offset-to-depth-ratio for the bottom of the reservoir reaches only 1.6 in the center of the study area and decreases toward the edges, the anellipticity parameters $\eta^{(1,2,3)}$ may not be tightly constrained. The performance of MASC, however, is not strongly influenced by trade-offs between the moveout parameters, as long as the moveout equation gives an accurate approximation for the traveltime surface (Xu and Tsvankin, 2006a). The high quality of the traveltime fit provided by our moveout-inversion algorithm is confirmed by the large semblance values (0.7 on average) for the bottom of the reservoir.

Correlation between the NMO and AVO ellipses. It has been suggested in the literature that combining the NMO ellipse with the azimuthally-varying AVO gradient can help to constrain the anisotropic velocity model and some physical fracture parameters (Rüger and Tsvankin, 1997; Bakulin et al., 2000). This approach is feasible when the reservoir is thick enough for reliable estimation of the interval NMO ellipses, and the variation of major fracture properties (orientation, density, fluid saturation) with depth is not significant. In the presence of strong vertical heterogeneity, the difference in vertical resolution between amplitude and traveltime methods complicates joint analysis of AVO and NMO results.

Although the thickness of the reservoir formation at Rulison is sufficient for azimuthal moveout inversion, there is no obvious correlation between the azimuthal NMO and AVO attributes. Most likely, the vertical and lateral heterogeneity of the Williams Fork Formation has a strong impact on the interval NMO ellipses, which reflect the average properties of the reservoir. In contrast, azimuthal AVO response after the geometrical-spreading correction mostly depends on the local medium properties above and below the reflector. Still, further joint analysis of the NMO and AVO attributes may be helpful in improving our understanding of the reservoir.

Quantitative AVO inversion. The AVO gradient is estimated here by expressing the reflection coefficient as a quadratic function of the source and receiver coordinates. While this representation is justified for the NMO ellipse (Grechka and Tsvankin, 1998), it is not appropriate for quantitative inversion of the AVO response. Indeed, the plane-wave reflection coefficient obtained by amplitude processing has to be treated as a function of the incidence phase angle or horizontal slowness (ray parameter). Accurate computation of the phase angle at the reflector, however, requires knowledge of the interval anisotropy parameters in the overburden. Also, the reconstructed reflection coefficient has to be calibrated using borehole information (well logs). Additional complications in AVO inversion at Rulison may be caused by the presence of multiple fracture sets (Vasconcelos and Grechka, 2007). These issues deserve further investigation, which is outside of the scope of this paper.

Conclusions. Despite the complexity of the heterogeneous fractured reservoir in the Rulison Field, P-wave reflection data provide valuable information for fracture characterization. Our processing sequence included advanced anisotropic traveltime and amplitude inversion methods designed for wide-azimuth, long-offset data. Nonhyperbolic moveout analysis for several major horizons helped to flatten the long-spread reflection events and estimate the effective NMO ellipses and η-parameters. Then the generalized Dix equation was used to

remove the influence of the overburden and compute the interval NMO ellipses in the reservoir and the layer above it (UMV shale). The estimated nonhyperbolic moveout parameters also provided the input to the moveout-based anisotropic geometrical-spreading correction (MASC), which was applied prior to azimuthal AVO analysis. The azimuthal variation of the AVO gradient (AVO ellipse) proved to be the most sensitive fracture-detection attribute. Significant azimuthal AVO anomalies were observed for all three processed horizons, which indicates that fracturing is not limited to the reservoir formation. It should be emphasized that the AVO response for the bottom of the reservoir is substantially distorted by the azimuthally varying geometrical spreading. The AVO-gradient anomaly in the lower left corner of the study area becomes much more pronounced and spatially coherent after application of MASC. It is clear that an accurate spreading correction is even more important for quantitative inversion of the azimuthal AVO attributes. Note that implementation of MASC is entirely based on the results of azimuthal moveout analysis and, therefore, involves almost no extra computational cost.

The two strong AVO-gradient anomalies at the bottom of the reservoir coincide with the intersections of wrenching fault systems, where one can expect concentration of stress. While the fracture orientation estimated from the AVO ellipses varies over the field, the dominant fracture azimuth (N70W) is in good agreement with EMI logs and the direction of one of the fault systems. This geologic evidence suggests that the anomalies indeed correspond to "soft spots" of high fracture density.

The interval NMO ellipticity in the reservoir is much less pronounced compared to the azimuthal variation of the AVO gradient for the reservoir boundaries. Also, the azimuthal AVO and NMO attributes are not well correlated, which may be explained by the inherent difference between these two measurements. Reflection coefficient is governed by the local contrasts in the elastic parameters across interfaces, whereas NMO velocity reflects the average medium properties over coarse intervals. Since the reservoir horizon at Rulison is thick and heterogeneous, the weak correlation between the AVO and NMO ellipses is not surprising.

Suggested reading. "Estimation of fracture parameters from reflection seismic data—Parts I and II" by Bakulin et al. (GEOPHYSICS, 2000). "Geology of the basin-centered gas accumulation, Piceance Basin, Colorado" by Cumella and Ostby (*Piceance Basin 2003 Guidebook*, Rocky Mountain Association of Geologists, 2003). "3D description of normal moveout in anisotropic inhomogeneous media" by Grechka and Tsvankin (GEOPHYSICS, 1998). "3D moveout inversion in azimuthally anisotropic media with lateral velocity variation: Theory and a case study" by Grechka and Tsvankin (GEOPHYSICS, 1999). "Generalized Dix equation and analytic treatment of normal-moveout velocity for anisotropic media" by Grechka et al. (*Geophysical Prospecting*, 1999). "Fracture detection using 3D azimuthal AVO" by Gray and Todorovic-Marinic (*CSEG Recorder*, 2004). "Fracture characterization at Valhall: Application of P-wave amplitude variation with offset and azimuth (AVOA) analysis to a 3D ocean-bottom data set" by Hall and Kendall (GEOPHYSICS, 2003). "Seismic investigation of wrench faulting and fracturing at Rulison Field, Colorado" by Jansen (Master's thesis, Colorado School of Mines, 2005). "P-wave and S-wave azimuthal anisotropy at a naturally fractured gas reservoir, Bluebell-Altamont Field, Utah" by Lynn et al. (GEOPHYSICS, 1999). "Fracture characterization of deep tight sands using azimuthal velocity and AVO seismic data in Saudi Arabia" by Neves et al. (*TLE*, 2003). *Reflection Coefficients and Azimuthal AVO Analysis in Anisotropic Media* by Rüger (SEG, 2001). "Using AVO for fracture detection: Analytic basis and practical solutions" by Rüger and Tsvankin (*TLE*, 1997). "Azimuthal variation in AVO response for fractured gas sands" by Sayers and Rickett (*Geophysical Prospecting*, 1997). *Seismic Signatures and Analysis of Reflection Data in Anisotropic Media* by Tsvankin (Elsevier, second edition, 2005). "Seismic characterization of multiple fracture sets at Rulison Field, Colorado" by Vasconcelos and Grechka (GEOPHYSICS, 2007). "Nonhyperbolic moveout inversion of wide-azimuth P-wave data for orthorhombic media" by Vasconcelos and Tsvankin (*Geophysical Prospecting*, 2006). "Geometrical spreading of P-waves in horizontally layered, azimuthally anisotropic media" by Xu et al. (GEOPHYSICS, 2005). "Anisotropic geometrical-spreading correction for wide-azimuth P-wave reflections" by Xu and Tsvankin (GEOPHYSICS, 2006a). "Azimuthal AVO analysis with anisotropic spreading correction: A synthetic study" by Xu and Tsvankin (*TLE*, 2006b). TLE

Acknowledgments: We are grateful to Tom Davis, Bob Benson, Michael Rumon, Eldar Guliyev, and Matthew Casey from the Reservoir Characterization Project (RCP) at CSM for providing the seismic data and valuable additional information for this study. We thank our colleagues at the Center for Wave Phenomena (CWP), in particular Ken Larner, Ivan Vasconcelos, Carlos Pacheco, Rodrigo Fuck, Jyoti Behura, and John Stockwell, for stimulating discussions and technical help. Shannon Higgins (RCP, now Schlumberger) helped us with the image logs and Kjetil Jansen (RCP, now Occidental) shared his fault maps. The support for this work was provided by the Consortium Project on Seismic Inverse Methods for Complex Structures at CWP and by the Chemical Sciences, Geosciences and Biosciences Division, Office of Basic Energy Sciences, Office of Science, U.S. Department of Energy. Xiaoxia Xu is now with ExxonMobil Upstream Research Company.

Corresponding author: ilya@dix.mines.edu